Online ISSN: 2981-0396 Print ISSN: 2981-0388

International Journal of Iron & Steel Society of Iran

Journal Homepage: https://journal.issiran.com/

Research Article

Canola Meal–Derived Biochar as a Renewable Carbon Source for Reducing Fossil Carbon Use and Greenhouse Gas Emissions in Ferrosilicon and Iron Production

R. Amini Najafabadi *[1], A. Rabiee [2], S. E. Aghili [3]

Materials Engineering Group, Golpayegan College of Engineering, Isfahan University of Technology, Golpayegan, Iran

ARTICLE INFO

Keywords:

Canola, Biochar, Carbon, Greenhouse, Iron Production.

Article history:

Received 15 December 2025
Received in revised form 30 December 2025
Accepted 17 May 2026

ABSTRACT

This study investigates the feasibility of using canola meal as a feedstock for biochar production. After drying and milling, the samples were subjected to slow pyrolysis at 350 and 500°C, and the physicochemical properties of the resulting biochars were characterized using CHNS, FTIR, Raman spectroscopy, TG/DTG, and DSC analyses. CHNS results showed that the biochar produced at 350°C contained 48.75% carbon and exhibited a higher H/C ratio compared to the 500°C sample, indicating the presence of remaining organic compounds and a less aromatic structure. FTIR analysis confirmed the reduction of C=C bands and the increase of carbonyl groups with rising temperature. Raman spectra revealed that the carbon structure of the 350°C biochar was predominantly amorphous (D1 type), with an increased ID/IG ratio reflecting greater structural disorder induced by pyrolysis. TG/DTG and DSC results demonstrated that the canola meal biochar possesses suitable thermal stability, requiring lower thermal degradation energy than fossil carbon materials. Considering its carbon content, negligible sulfur level, and favorable thermal resistance, canola meal can serve as a sustainable and renewable source for biochar production and a partial substitute for fossil carbon in metallurgical industries such as ferrosilicon and direct-reduced iron production.

1. Introduction

Fossil fuels used in steel and iron production can be replaced with biochar and coke [1]. Greenhouse gas emissions can be reduced through the potential of these materials [2, 3]. Biocarbon resources must possess several specific characteristics, including abundance and renewability, to sustainably meet the needs of industries such as steel. In addition, they must be cost-effective and should not increase the cost of producing carbon materials. Besides, environmental protection should be regarded as a primary issue, and harvesting forest resources toned to consider the consequences of environmental damage and destruction [4-6]. Previously, industries such as ferroalloys and ferrosilicon used coal from sawmill chips alongside fossil coke, in both composite and separate forms [7], leading to improvements in the production process and a higher quality of silicon and silica products. Another benefit of using biochar is the reduction in emission indices of pollutant gases such as carbon dioxide and sulfur dioxide [4]. For example, the potential of biochar for application in ferromanganese production was demonstrated by Sorp et al. [8], who performed their investigation from a life cycle assessment (LCA) perspective. Their findings revealed that bio-based metal reductants could significantly reduce greenhouse gas

* *Corresponding Author*
Email: r.amini@iut.ac.ir
Address:Materials Engineering Group, Golpayegan College of Engineering, Isfahan University of Technology, Golpayegan, Iran
1. Associate Professor, 2. M.S.c, 3. Assistant Professor

DOI: http://10.22034/IJISSI.2026.2080945.1342
Published by ISSI (Iron & Steel Society of Iran)

emissions in the ferromanganese production process. Graphite electrodes in electric arc furnaces, biochars, and cathode graphite linings are among the components involved in the Hall–Héroult process for aluminum extraction from biochar consumption positions [9].

The properties of several charcoals produced from various raw materials have been evaluated [10, 11]. Several methods, such as torrefaction [12] and Pyrolysis [13, 14], are also available for producing charcoal. These processes have been exmained for their ability to create a variety of properties and products (solid, liquid, and gas) [15, 16].

Charcoal production by slow pyrolysis method [17] offers the highest yield of solid carbon material compared to fast and medium pyrolysis. Several parameters influence the quantitative and qualitative properties of the resulting charcoal, including pyrolysis temperature[18] residence time [19], heating rate (°C/min) [20], and the biomass composition in terms of carbon content, ash, and volatile matter [21, 22]. It has been shown that the carbon concentration in coal increases at higher pyrolysis temperatures, as demonstrated through tests at various temperature levels. The study by Femi et al. [18] revealed that increasing the pyrolysis temperature from 400 to 800°C raised the carbon concentration of coal from 82.74 ± 0.07 to 96.1 ± 0.02 percent, although the process efficiency decreased from 39% to 27%. Zhao et al. also reported that changing the duration of raw material storage in the furnace from 10 to 100 minutes increased the carbon concentration of biochar from 74.53 to 77.12%. Engine [20] found that increasing the heating rate from 10 to 50°C/min raised the carbon concentration from 67.30 to 71.70, which is associated with the release of volatile compounds. Biochar has a wide range of applications, including the improvement of soil's physical and chemical properties [23]. The effect of biochar on gas purification has also been investigated by Lehman et al.[24] , who used charcoal odor to reduce H_2S gas.

Rapeseed oil is an important agricultural product obtained from the compression of canola seeds and is the second most widely cultivated oilseed in the world after soybeans [25]. The by-products of rapeseed oil extraction, produced in large quantities, are primarily utilized for fuel, fertilizer, and animal feed [26]. However, due to the presence of potentially harmful substances in these residues[27], their usage in animal feed must be limited. Such limitations contribute to the disposal of substantial volumes of oilseed waste, including residues from rapeseed, soybean, sunflower, etc.

Given the large amount of oilseed meal production, this study has investigated the properties of rapeseed meal as a raw material for biochar production. For this purpose, a series of proximate and ultimate analyses were conducted, along with advanced characterization techniques including Fourier-transform infrared (FTIR) spectroscopy, Raman spectroscopy, thermogravimetric/ differential thermogravimetric (TG/DTG) analysis, and differential scanning calorimetry (DSC), to determine the structural and thermal properties of pyrolyzed rapeseed meal charcoal.

2. Materials and Methods

A total of 1000 grams of rapeseed was prepared and subjected to at a temperature of 49°C and a constant pressure of 0.9 Pa. The resulting meal was collected in briquetted form and subsequently crushed and sieved to a particle size of approximately 200 µm according to ASTM D 1762-84 standards. A sample of rapeseed meal (RM) briquettes was weighed (36 grams) using an analytical balance with a precision of 0.000 g and dried in a ceramic crucible (50 cc capacity) at 105°C for 24 hours. Proximate analysis was conducted to determine the moisture content (in an oven at 105°C), ash content (muffle furnace at 500°C), and volatile matter (in a muffle furnace at 900°C), according to the ASTM D1102-84 standard. The analysis was repeated three times, and average values were calculated based on the weight measurements before and after heating in the muffle furnace. A 35-gram sample of rapeseed meal charcoal was subjected to slow pyrolysis to produce charcoal in an oxygen-free atmosphere. The temperature was gradually increased at a rate of 10°C/min until reaching 350°C. The obtained charcoal powder was named (RM350). FTIR analysis was conducted on the dry meal sample (RM105) and pyrolyzed charcoal samples (RM350 and RM500), using 0.2 g of each material and a Bruker instrument. CHNS analysis was performed following ASTM D3176-89 and using a PerkinElmer 2400 analyzer to determine the carbon, hydrogen, and nitrogen contents of the pyrolyzed charcoal. Raman analysis was performed using a Thermo Scientific Nicolet device in the spectral range of 400-2000cm^{-1} to determine the changes in meal and coal more accurately. The thermal properties of meal and coal were investigated using TG/DTG analysis with a METTLER TOLEDO device. Samples were placed in an alumina sample container in the temperature range of 25-1000°C and a heating rate of 10°C/min under a nitrogen atmosphere at a rate of 50 mL/min, with a target temperature of 453°C. Thermal changes (endothermic and exothermic reactions) were investigated using DSC calorimetry in the temperature range of 25-453°C, under identical heating and nitrogen flow conditions, with a DSC302 device.

3. Results and Discussion

3.1. CHNS Analysis

Table 1. shows the results of the carbon, hydrogen, nitrogen and sulfur content of the pyrolyzed coal sample RM350 determined by CHNS analysis, along with the molar mass ratio of hydrogen to carbon. Another sample (RM500) was also prepared under slow pyrolysis conditions at 550°C. The carbon content of the primary sample under investigation (RM350) was 48.75%. On the other hand, the two additional tested samples had

carbon contents of 50% and 53.6%, respectively. These differences could be associated with the quality of the grain, the type of oiling process, and the content of other nitriding and hydrocarbon compounds. The hydrogen-to-carbon ratio in the rapeseed meal sample (RM350) was higher than that of the RM500 sample, reflecting a greater hydrogen content in RM350. Given the known concentrations of C, H, N, and ash, the maximum heat production value of the fuel can be calculated using Eq.(1), as proposed by Channiwala [28].

$$HHV=0.3491C\%+1.1783H\%+0.1005N\%-0.1034O\%-0.0211ash \quad \text{Eq.(1)}$$

The HHV comparison indicates that the HHV of coal decreases with increasing pyrolysis temperature (e.g. 650°C). It is suggested that by reducing the temperature, duration, and heating rate during pyrolysis, metal reduction processes can be facilitated using the gases produced (H_2, CO, CO_2, CH_4), which are stored in pyrolysis process tanks [29]. It is possible to use these gases in the direct reduction reactions involved in green steel production. The low HHV value limits the effectiveness of biochar for heat generation. However, an important advantage of biochar over coal is its negligible sulfur content, which addresses impurity-related hazards. Beyond the problems of coal usage, including its conversion into coke and the limitations of fossil resources, biochar has various environmental and practical advantages.

Chaniwala et al. [28] examined several bio-based feedstocks (coconut shell, peanut shell, etc.) for their elemental composition. The RM350 sample demonstrated a carbon concentration close to that of the peanut shell (Table 1.). The hydrogen content of RM350 is approximately twice that of peanut shell, which raises the possibility of higher energy release during combustion. In addition, oilseed meals, such as rapeseed, offer more sustainable and abundant sources. On the other hand, rice husk combustion causes considerable greenhouse gas emissions. Oni et al. [30] examined various biomass-derived charcoals, including rice husk charcoal, wood husk charcoal, sugar beet meal charcoal, poo chips, and cow and chicken manure. According to the analysis results, the carbon concentration in the charcoals varied depending on the pyrolysis temperature, ranging from 49% to 93%, while the hydrogen concentration ranged from 2.6% to 3.6%. Sun et al.[29] used different temperature conditions and heating rates for the pyrolysis of rapeseed meal. The highest charcoal yield was obtained under slow pyrolysis conditions at 350°C with a low heating rate of 5 K/min, whereas the maximum carbon concentration was produced in the sample pyrolyzed at 650°C with medium heating rate (24.1K/min) (Table 1). The pyrolysis temperature of 350°C was selected for this study because of its high efficiency and lower energy consumption during the charcoal production process.

Table 1. Elemental Composition (C, H, N, S) of Pyrolyzed Charcoal Sample RM350.

	C	H	N	S	H/C	HHV(KJ/Kg)
RM350	48.75	11.39	4.58	<0.1	2.8	27.4
350°C-S[29]	50.0	9.1	9.3		2.2	25.5
650°C-S[29]	53.6	6.8	9.5		1.5	24.9
650°C-M[29]	52.7	7.9	7.9		1.8	26
COAL(Blue Gem)[31]	80.5	5.29	1.98	0.73		
Peak Downs[31]	77.1	4.34	1.68	0.58		
Groudnut shell[28]	48.59	5.64	0.58			19.698
673.15 K[32]	61.8	2.54	7.12			
Pine-raw[33]	48.23	6.15	0.13	0	1.53	19.48
Pine -550[33]	67.55	2.82	0.41	0.01	0.5	24.60
P4-L1-550[33]	71.38	2.41	0.31	0.96	0.4	26.32
Coke[34]	83.36	1.14	0.39	0.30		
Palm char[34]	59.35	2.98	0.30			

Mirogens et al. [31] used various carbon sources such as coal, coke, charcoal, wood chips, and biochar to produce metallic silicon. The researchers examined the relationship between charcoal reactivity and porosity, reporting fixed carbon contents ranging from 59% to 67% in the minimum and maximum states. The carbon concentration in the final analysis was 80.5 and 75.9% by weight. High reactivity, high conversion rate, and negligible impurity were mentioned as important characteristics of carbon materials. Noteworthy, biochar exhibited negligible sulfur content, while this element was present in coal and coke at 0.73 and 0.58%, respectively. The presence of sulfur pollutant and its potential removal by biochar can be regarded as key environmental considerations.

Noorfarhana et al.[34] investigated the combination of palm charcoal, Fe_2O_3, SiO_2, and coke in specific ratios in the process of ferrosilicon synthesis. The results showed that the silicon concentration was 41.14% higher when coke was used as the carbon source compared to palm charcoal, although the reduction efficiency of silica was superior with palm charcoal.

3.2. FTIR

FTIR spectroscopy was performed to investigate the functional groups present in biomass and biochar samples. Simplicity, non-destructiveness, speed, and accuracy are the main characteristics of this analysis. FTIR spectroscopy was performed in the range of absorbed spectra 400-4000cm^{-1}, enabling the identification of chemical compounds and functional groups. In addition, the differences in wave absorption values by biomaterial and charcoal, along with the changes caused by the key pyrolysis parameters (temperature, residence time and heating rate) were also evaluated Fig. 1. presents the FTIR spectra of the raw material, rice bran dried at 105°C, and biochar samples pyrolyzed at 350 and 500°C. Sun et al. [29] reported six main groups with high absorption intensity in the infrared spectrum. These observations included the –OH stretching vibration at 3400cm^{-1}, C–H vibrations (CH_3, CH_2) at 2920cm^{-1}, stretching vibrations of C=C and C=O at 1646cm^{-1}, C=C vibrations associated with aliphatic chains (CH_3, CH_2) at 1455cm^{-1}, and C–O–C and Ar–H stretching vibrations at 1050cm^{-1} and 787cm^{-1}, respectively. Structural changes induced by pyrolysis conditions can be evaluated by examining the absorption values of C=O and C=C and their ratios. Consistent with the results of the above study, a decrease in the C=O/C=C ratio was reported with increasing pyrolysis temperature from 350°C to 500°C and 650°C. The FTIR analysis results of RM105, RM350, and RM500 also confirmed this decreasing trend from 350°C and 500°C, whereas the dry powder sample and the RM350 biochar exhibited a relatively higher C=O/C=C ratio. Fig. 2. shows the changes in infrared absorption associated with C=C stretching vibrations during the pyrolysis of the rapeseed meal. These vibrations exhibited less infrared absorption at higher pyrolysis temperatures. Since the infrared absorption and the amount of compound present in the sample are directly related, it is observed that increasing the pyrolysis temperature from 350°C to 500°C has caused the decomposition and elimination of C=C bonds. In the case of C=O stretching vibrations, increasing temperature increases infrared absorption, suggesting that C=O vibrations are formed as a result of pyrolysis and increasing pyrolysis temperature (Fig. 3.).

The observed decrease in C=C stretching vibrations and the corresponding increase in C=O stretching vibrations during pyrolysis at 350°C indicate that this temperature can be sufficient for coal pyrolysis.

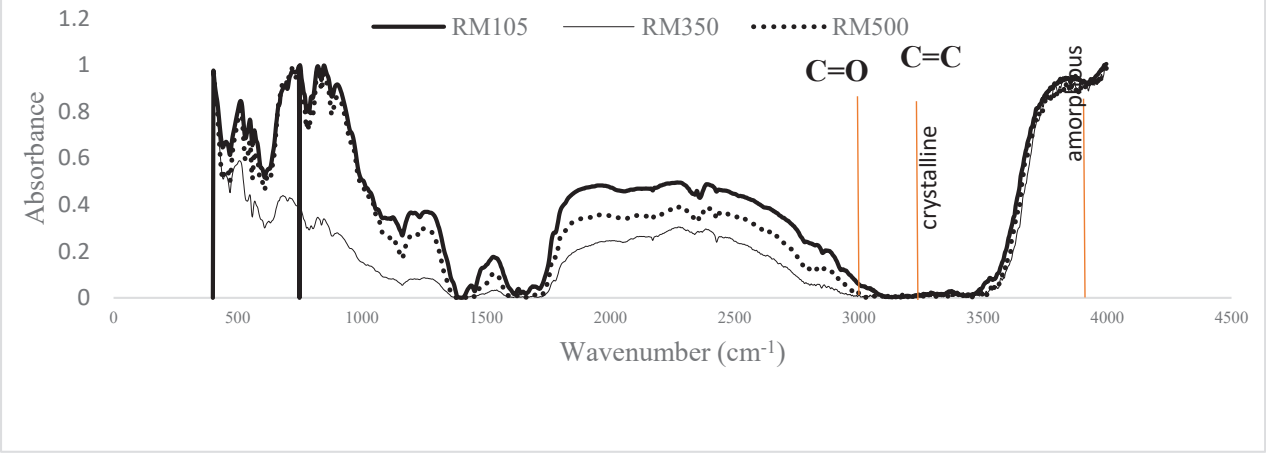

Fig. 1. FTIR spectra showing infrared absorption characteristics of dried RM105 raw material and biochar pyrolyzed at different temperatures in the range of 400-4000cm^{-1}.

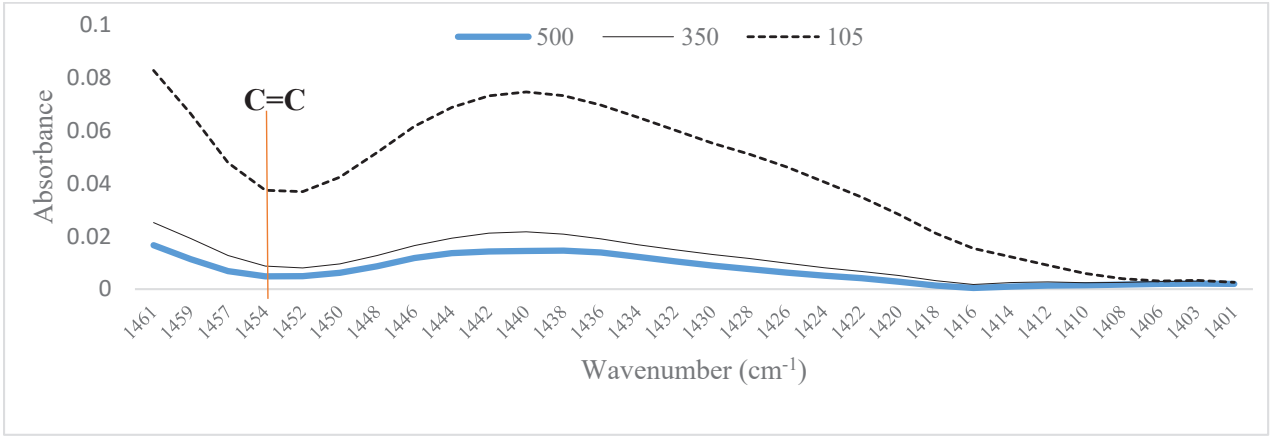

Fig. 2. FTIR spectra highlighting infrared absorption changes associated with C=C stretching vibrations in dried RM raw material and biochar pyrolyzed at different temperatures in the range of 1401-1461cm^{-1}.

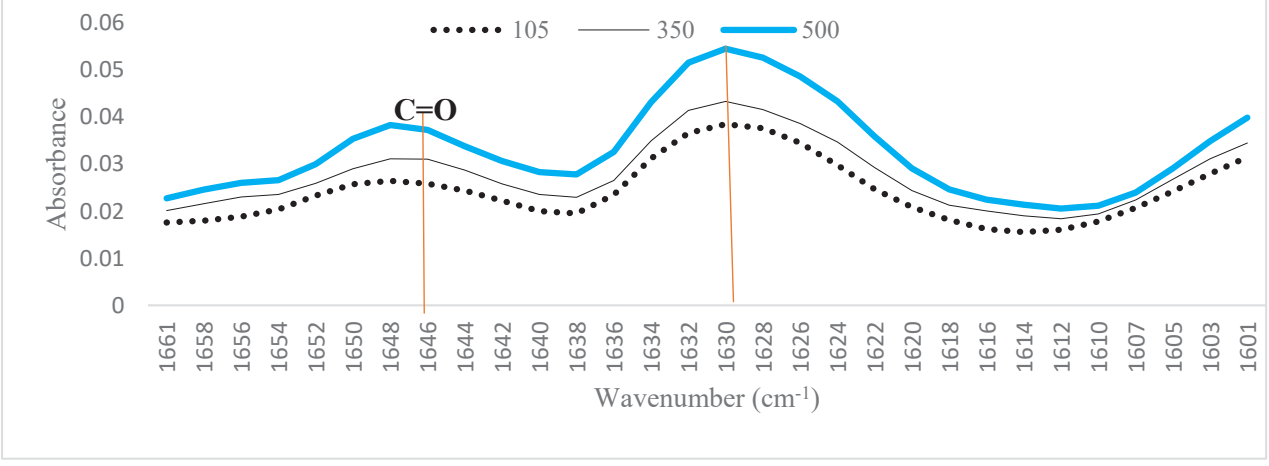

Fig. 3. FTIR spectra indicating infrared absorption changes associated with C=O stretching vibrations in dried RM raw material and biochar pyrolyzed at different temperatures in the range of 1601-1661cm^{-1}.

Chow et al. [35] identified the 1623cm^{-1} band as indicative of moieties containing the crononyl group. The increase in IR absorption by this moiety in the RM350 sample was relatively minor and remained stable at a pyrolysis temperature of 350°C. The stability of this moiety was also recorded at 700°C, which highlights its thermal resilience under different thermal conditions. As the pyrolysis temperature increased from 105°C to 550°C, the aromatic CH nuclei in the range of 800-880cm^{-1} recorded an increase in absorption. In addition, the 1100-1300cm^{-1} range belonging to hydroxybenzene (C-O, C-C, -OH) also increased, with the highest absorption peak recorded at 1279cm^{-1}. Song Yan et al. [36] reported the range of 900-1375cm^{-1} as being highly dependent on the crystalline and amorphous regions. Their findings indicated that the addition of NaOH caused a decrease in the absorption in the 1430 cm^{-1} band, which belongs to the crystalline region, and an increase in the ~897cm^{-1} band, which belongs to the amorphous structure. The absorption by this band (~900cm^{-1}) in the RM550 sample is much higher than that of RM350, demonstrating that the amorphous structure (cellulose) has increased at higher pyrolysis temperatures. The crystalline and amorphous levels of the structure are evaluated through the crystallinity index (CI = A1430/A897). A1430 and A897 represent the infrared absorption intensities corresponding to the characteristic crystalline and amorphous bands, respectively. The CI values calculated as the ratio A1430/A897 for the RM350 and RM550 samples were 1.03% and 1.50%, respectively.

Bin Gong [37] reported that strong infrared absorption was observed at 2920cm^{-1} and 3050cm^{-1}, corresponding to aliphatic C–H stretching vibrations in cellulose and aromatic C–H stretching in lignin, respectively. This study indicated that cellulose was not completely carbonized by pyrolysis. In the case of the meal charcoal sample, the changes of this band were insignificant. Huikeng [38] reported that infrared absorption bands at 3041cm^{-1} and 2905cm^{-1} correspond to NH_4^+ and NH_2 functional groups, respectively. CHNS analysis reported the presence of high amounts (4.58%) of C-H-N.

The infrared absorption intensities at 2905cm^{-1} and 3041cm^{-1} in the charcoal sample were significantly reduced compared to those in the dried powder due to pyrolysis.

3.3. Raman

Raman spectroscopy shares several similarities with FTIR, although there are two fundamental differences between the two techniques. The first difference lies in the fact that Raman uses two photons, but FTIR uses one [39]. Second, Raman uses the scattering of light by frequency changes caused by the reduction or absorption of vibrations by the molecules of the material, while FTIR uses the peaks with the maximum energy of Rayleigh waves.

Carbon exists in seven distinct structural forms, including diamond, hexagonal diamond, graphite and graphene, amorphous carbon, single-walled carbon nanotubes, carbon nanofibers, and glassy carbon. Ferrari et al. [40] investigated the structures of amorphous carbon D and graphite G using Raman analysis. The study employed the intensity ratio of the D to G bands (I_D/I_G) to assess the degree of disorder in carbon structures, particularly in dried and pyrolyzed samples at 350°C, following Gavilian et al. [41]. The broad Raman band at 1580cm^{-1} corresponds to the G band and is indicative of graphite with an ideal lattice. The D1 and D2 bands (graphite with a disordered structure) are identified at 1350cm^{-1} and 1620cm^{-1}, respectively. In addition, the 1520cm^{-1} and 1260cm^{-1} peaks correspond to D3 (amorphous carbon) and D4 (disordered graphite structure) structures.

As shown in Fig. 4. Raman spectrum analysis of the dried rapeseed meal powder sample revealed seven peaks with the highest absorption at 3866, 2922, 1909, 1855, 1724, 1635, and 1597cm^{-1}, respectively.

Fig. 4. shows the Raman spectroscopy of a sample of rapeseed meal dried at 105°C (RM105), with absorption intensities for the G, D1, D2, D3, and D4 bands presented in Table 2. The Raman absorption in peak G of RM105 was the highest (G>D2>D3>D4>D1), and the ratio ID(D1+D2)/IG=1.69 was also calculated. On the other hand, Fig. 5. shows the Raman spectrum of the pyrolyzed sample at 350°C (RM350), indicating a higher degree of structural disorder for the I_D/I_G ratio increased to 2.25. In RM350, the highest infrared absorption was by D4, and the absorption values generally decreased compared to RM105. The relative absorption values changed as D4<D1<D3<D2 due to the decomposition

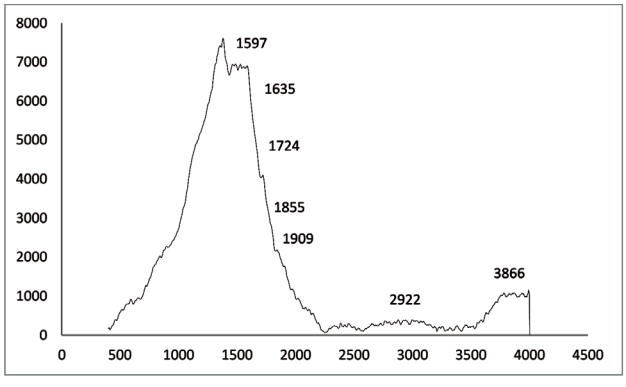

Fig. 4. Raman spectroscopy of dried powder at 105°C.

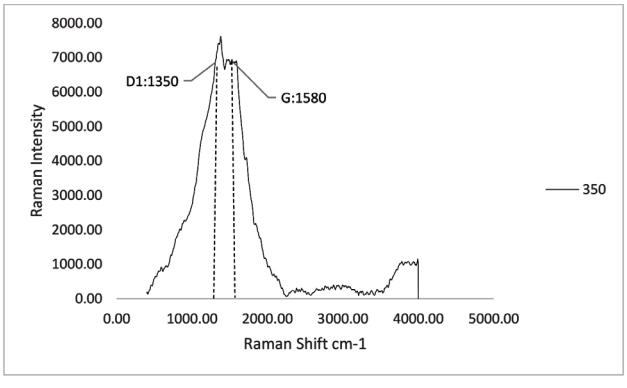

Fig. 5. Raman spectroscopy of pyrolyzed biochar at 350°C.

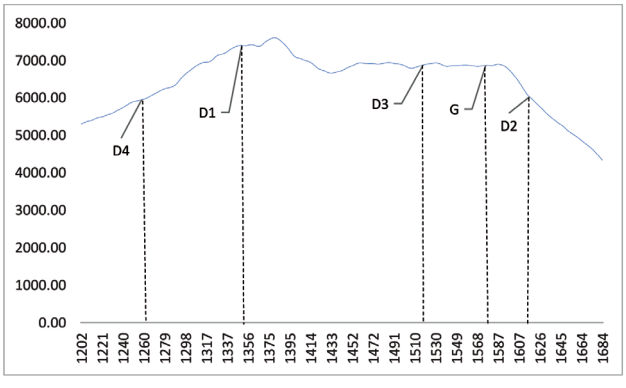

Fig. 6. Raman spectroscopy of pyrolyzed biochar at 350°C in the spectral range of 1201-1683 cm^{-1}.

and compounds resulting from pyrolysis. The ID/IG ratio of the pyrolyzed sample reveals that pyrolysis has caused a structural change from relatively regular to disordered and amorphous structures. Fig. 6. provides a detailed view of the absorption peaks of RM350. As reported by Sparavigna [41], the peak at 1387cm^{-1} (Fig. 6.), indicated an absorption intensity of 7508.58, reflecting disordered carbons. According to Fig. 6., the Raman absorption for D-carbon structures was in the order of D1>D3>D2>D4, suggesting D1 as the dominant structure in RM350 coal. The D2 structure, which had the maximum value in RM105, diminished significantly in RM350.

3.4. TG/DTG

Fig. 7. shows the changes in the reduced mass and thermal stability of rapeseed meal biochar during thermogravimetric analysis, conducted under ambient conditions with nitrogen gas flow and a heating rate of 10°C/min from 25 to 1000°C. The biomass is primarily composed of cellulose, hemicellulose, and lignin. Hemicellulose decomposes at 220-315°C, while cellulose decomposes at 315°C-400°C [42]. The thermal stability of lignin has been shown to remain stable from 150°C to 900°C. At temperatures below 200°C, cellulose, hemicellulose, and lignin are endothermic due to moisture loss. As the temperature increases to 355°C, cellulose continues to exhibit endothermic characteristics, while hemicellulose and lignin show exothermic responses at 275°C and 365°C, respectively.

Fig. 7a. shows the mass loss of biochar during TG analysis. At the onset of heating, the mass loss rate is initially low but becomes constant upon reaching a specific temperature threshold. The DTG curve in Fig. 7b. shows the initial stage of thermal degradation for rapeseed meal biochar, occurring between

Table 2. Raman absorption results by carbon modes RM105 and RM350.

Peaks	G	D1	D2	D3	D4	ID/IG
Absorb RM105	114367.5	70674.86	108475.5	108155.5	85509.63	1.69
Absorb RM350	5929.62	5987.22	7402.87	6905.59	6862.26	2.25

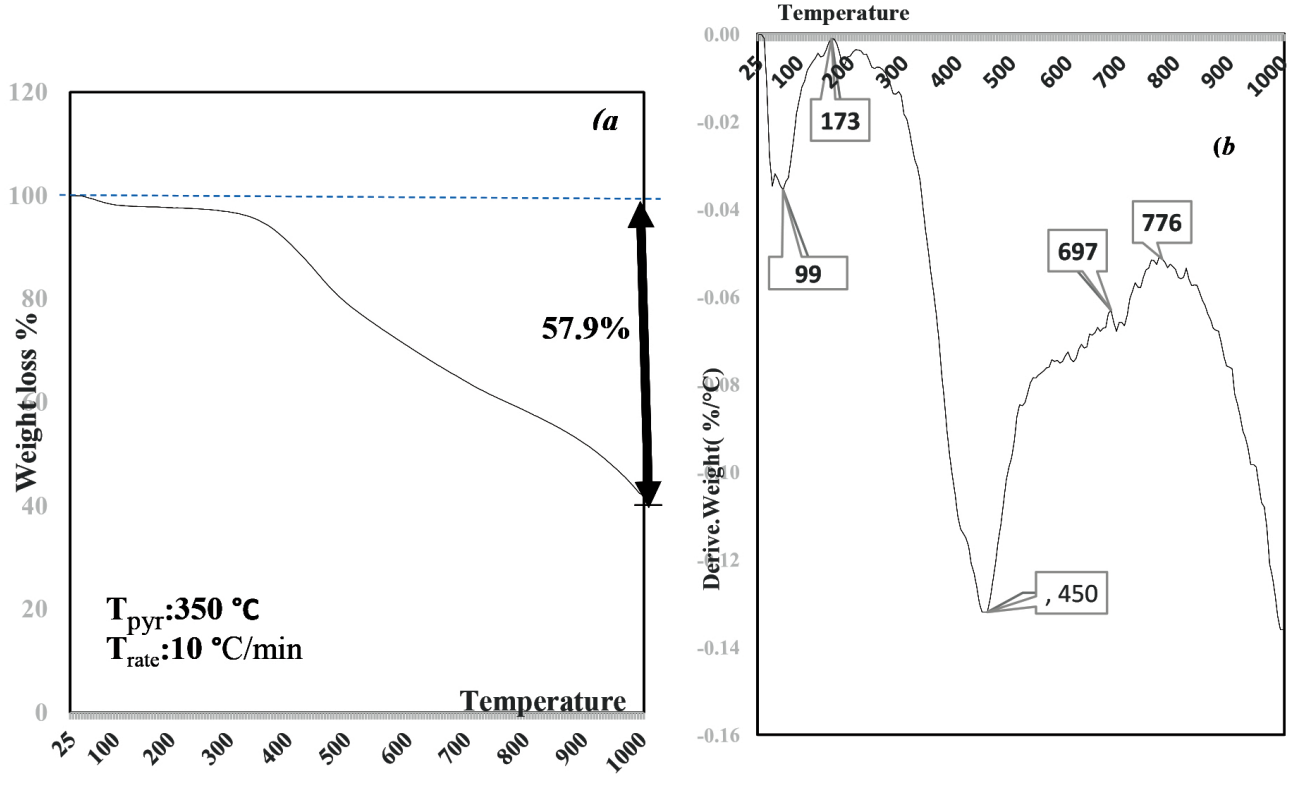

Fig. 7. TG and DTG curves of biochar pyrolyzed at 350°C at a heating rate of 10°C/min up to 1000°C in a nitrogen injection environment at a rate of 50 mL/min, a) TG and b) DTG.

25°C and 150°C. The maximum endothermicity is observed at a temperature of 99°C, which can be due to the evaporation of moisture, molecular water, and light volatile compounds, as well as the early thermal response of cellulose. The mass loss at this stage is 2.14%. There is no mass loss with the continued increase in temperature from 100°C to 311°C. Cellulose in the raw material is destroyed and decomposed when slow pyrolysis is performed at 350°C. In this range, the endothermic reaction changes to exothermic and reaches a maximum at 173°C. From 311°C to 450°C, a mass reduction gradient and a corresponding endothermic reaction occur in the coal, which is probably indicative of decomposition and destruction [43]. The original biomass is rich in protein, carbohydrates, and polyunsaturated fatty acids. Krzysztof Mazurek [32] reported that in the temperature range of 170°C -550°C the reaction energy would be exothermic, while an endothermic response was recorded between 170–450°C in the sample under study, which could be due to the difference in the pyrolysis temperature of coal. With the transition from 450°C, the reaction energy showed exothermic characteristics up to 776°C, after which the reaction energy showed endothermic behavior up to 1000°C. The mass reduction of the starting material was 57.9% at the end of the experiment, leaving 42.1% as residual biochar. The second stage of exothermicity was related to the breakdown of unstable oxygen-containing compounds (carboxyl and hydroxyl). In the third exothermic phase (450°C-770°C), the decomposition of nitrogen-containing compounds and the destruction of carbon materials were reported, leading to a mass reduction of 57.9%.

According to Yifan Sun [29], coal derived from slow pyrolysis exhibits lower thermal stability compared to that produced via medium pyrolysis. Biochar can be combined with fossil coke to form biocoke. Lichaw et al. [33] investigated the thermal behavior of biocoke using TGA and reported the intense reduction of the material at high temperatures, highlighting the importance of this characteristic in the reduction of iron oxides (conversion of Fe_2O_3 to Fe). They prepared samples of pine sawdust and lignin as pellets at 550°C for 1 h and a pressure of 10 MPa. The samples contained 48.23, 67.55, and 71.38% carbon, as indicated in Table 3. The drop in the TG curve at 520°C was attributed to the volatiles of lignin, cellulose, and hemicellulose that released water, aldehydes, phenols, and alcohols.

Here, T_i is the temperature at which volatiles begin to evaporate, T_{max} indicates the temperature at which the maximum weight loss of the material occurs during TG, and R_{max} indicates the maximum rate of material loss.

3.5. DSC

Fig. 8. shows the DSC differential scanning calorimetry curve of the dry powder and pyrolyzed carbon of rapeseed meal. The decomposition of cellulose is endothermic, while hemicellulose and lignin undergo exothermic decompositions [42]. DSC evaluates thermal stability primarily through two key parameters, including the peak height (mW) and the heat required for the reaction (j/g) [44].

Fig. 8. presents the initial thermal behavior of dry powder and charcoal samples during heating, where endothermic reactions could be observed. The highest amount of energy (endothermic) was close to -1.5Mw for the dry sample at 101°C, and −0.66 mW for the charcoal sample at 89°C. The evaporation of molecular moisture and volatiles can primarily illustrate the endothermic reactions. The increase in temperature causes a decrease in the endothermic energy and the start of exothermic reactions. The dry powder sample becomes exothermic upon reaching ~240°C, while it occurs at ~172°C for charcoal. This behavior is potentially associated with the decomposition and destruction of cellulose in the dry powder and its residues in the charcoal. The presence of exothermicity in the charcoal sample indicates the retention of volatile cellulose residues. The heating rate of 10°C/min is similar to the pyrolysis of the dry powder sample and the reactions that occur during pyrolysis. From 172°C to 185°C, the energy change is limited in coal, while the material undergoes a shift toward exothermic behavior with the temperature transition from 184°C, which is due to the decomposition and breakdown of hemicellulose and lignin bonds. At a temperature of ~432°C, the dry powder sample stops the increasing trend of the reaction energy TDSC = 432°C, DSCPEAK = 2.57mW, which does not occur for coal TDSC = 453°C, DSCPEAK = 2.84Mw. The enthalpy values of the reaction over the temperature range of ~250°C to 350°C at a heating rate of 10°C/min were 172 J/g for the dry powder and 129 J/g for the coal, which can be an estimate of the energy required for slow pyrolysis. The energy required to produce coal from biomass is less than that of fossil fuels [45].

Table 3. Temperature characteristics during TG.

Sample	Temperature (°C)		
	T_i	T_{max}	R_{max}
RM350	450	1000	-2.14
Pine-550 [33]	720	751	-3.5

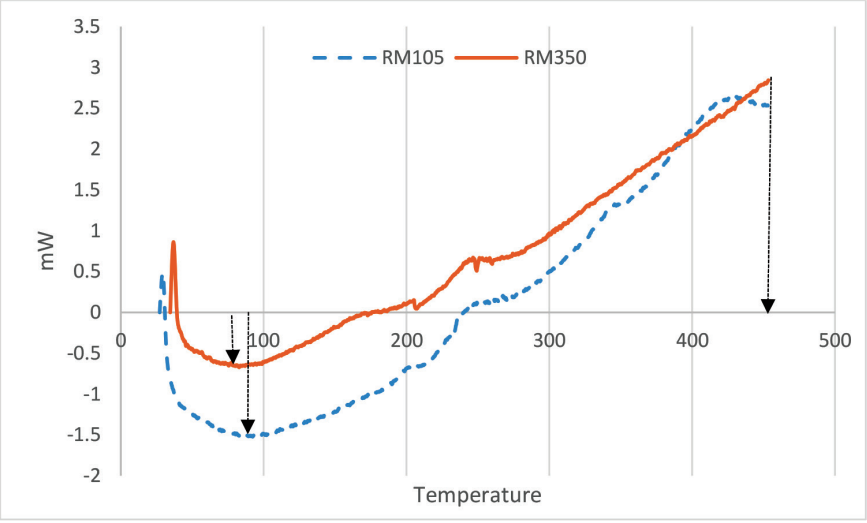

Fig. 8. Simultaneous DSC diagram of RM350 and RM105.

4. Conclusions

The physicochemical properties of biomaterials and the resulting charcoal were investigated using FTIR-Raman-TG/DTG-DSC analysis. Pyrolysis temperature, sample retention time at maximum temperature, and material type influence the properties of charcoal (regular or disordered amorphous graphite). The thermal stability and energy requirements for thermochemical decomposition and structural degradation during biochar production are lower than those needed for fossil-based carbon materials. Rapeseed meal exhibits high potential for carbonaceous charcoal production. The resulting biocarbonaceous charcoal can be used independently or composited with coal and fossil coke in industrial production of ferrosilicon and iron, consequently reducing the amount of fossil carbon. As demonstrated by structural analyses, the carbon structure in RM350 charcoal is of amorphous type D1 (graphite with disordered structure).

References

[1] Norgate T, et al. Biomass as a source of renewable carbon for iron and steelmaking, ISIJ Int. 2012; 52(8): 1472–1481.
[2] Jahanshahi S, et al. Development of low-emission integrated steelmaking process, J Sustain Metall. 2015; 1(1): 94–114.
[3] Jahanshahi S, et al. Biomass: providing a low capital route to low net CO_2. In: IEAGHG/IETS Iron and Steel Industry CCUS and Process Integration Workshop, 2013.
[4] Haque N, Norgate T, Estimation of greenhouse gas emissions from ferroalloy production using life cycle assessment with particular reference to Australia, J Clean Prod. 2013; 39: 220–230.
[5] Sommerfeld M, Friedrich B, Replacing fossil carbon in the production of ferroalloys with a focus on bio-based carbon: a review, Minerals. 2021; 11(11): 1286.
[6] Grønnli M, et al. The use of biocarbon in Norwegian ferroalloy production, Infacon. 2001; 9: 268–276.
[7] Surup G.R, Trubetskaya A, Tangstad M, Life cycle assessment of renewable reductants in the ferromanganese alloy production: a review, Processes. 2021; 9(1): 185.
[8] Dall'Osto G, et al. Biochar and other carbonaceous materials used in steelmaking: possibilities and synergies for power generation by direct carbon fuel cell, Biomass Bioenergy. 2023; 177: 106930.
[9] Conz R.F, et al. Effect of pyrolysis temperature and feedstock type on agricultural properties and stability of biochars, Agric Sci. 2017; 8(9): 914.
[10] Han Y, Tangstad M, Metallurgical properties of biocarbon in ferroalloy production: a review, ACS Omega. 2024; 9(23): 24142–24162.
[11] Krysanova K, Krylova A, Zaichenko V, Properties of biochar obtained by hydrothermal carbonization and torrefaction of peat, Fuel. 2019; 256: 115929.
[12] Crombie K, et al. The effect of pyrolysis conditions on biochar stability as determined by three methods, GCB Bioenergy. 2013; 5(2): 122–131.
[13] Garcia-Perez M, Lewis T, Kruger C, Methods for producing biochar and advanced biofuels in Washington State, Part 1. 2010: 137.
[14] Meyer S, Glaser B, Quicker P, Technical, economical, and climate-related aspects of biochar production technologies: a literature review, Environ Sci Technol. 2011; 45(22): 9473–9483.
[15] Brown R, Biochar production technology, In: Biochar for environmental management. Routledge. 2012: 159–178.
[16] Al-Rumaihi A, et al. A review of pyrolysis technologies and feedstock: a blending approach for plastic and biomass towards optimum biochar yield, Renew Sustain Energy Rev. 2022; 167: 112715.

[17] Titiladunayo I.F, McDonald A.G, Fapetu O.P, Effect of temperature on biochar product yield from selected lignocellulosic biomass in a pyrolysis process, Waste Biomass Valor. 2012; 3: 311–318.
[18] Sun J, et al. Effects of pyrolysis temperature and residence time on physicochemical properties of different biochar types, Acta Agric Scand B Soil Plant Sci. 2017; 67(1): 12–22.
[19] Angın D, Effect of pyrolysis temperature and heating rate on biochar obtained from pyrolysis of safflower seed press cake, Bioresour Technol. 2013; 128: 593–597.
[20] Demirbaş A, Relationships between lignin contents and fixed carbon contents of biomass samples, Energy Convers Manag. 2003; 44(9): 1481–1486.
[21] Xiao R, et al. The physicochemical properties of different biomass ashes at different ashing temperature, Renew Energy. 2011; 36(1): 244–249.
[22] Devi P, Saroha A.K, Effect of pyrolysis temperature on polycyclic aromatic hydrocarbons toxicity and sorption behaviour of biochars prepared by pyrolysis of paper mill effluent treatment plant sludge, Bioresour Technol. 2015; 192: 312–320.
[23] Lehmann J, Joseph S, Biochar for environmental management: science, technology and implementation. 2024.
[24] Chauhan J, Choudhury P, Singh K, Production, varietal improvement programme and seed availability of annual oilseeds in India: current scenario and future prospects, J Oilseeds Res. 2021; 38(1): 1–18.
[25] Oskoueian E, et al. Bioactive compounds, antioxidant, xanthine oxidase inhibitory, tyrosinase inhibitory and anti-inflammatory activities of selected agro-industrial by-products, Int J Mol Sci. 2011; 12(12): 8610–8625.
[26] Chung K.T, Wei C.I, Johnson M.G, Are tannins a double-edged sword in biology and health? Trends Food Sci Technol. 1998; 9(4): 168–175.
[27] Channiwala S.A, Parikh P, A unified correlation for estimating HHV of solid, liquid and gaseous fuels, Fuel. 2002; 81(8): 1051–1063.
[28] Sun Y, et al. Pyrolysis behaviors of rapeseed meal: products distribution and properties, Biomass Convers Biorefinery. 2021; 1–16.
[29] Oni B.A, Oziegbe O, Olawole O.O, Significance of biochar application to the environment and economy, Ann Agric Sci. 2019; 64(2): 222–236.
[30] Myrvågnes V, Lindstad T, The importance of coal- and coke properties in the production of high silicon alloys, In: Innovations in Ferro Alloy Industry. 2007: 18–21.
[31] Mazurek K, et al. New separation material obtained from waste rapeseed cake for copper(II) and zinc(II) removal from the industrial wastewater, Materials. 2021; 14(10): 2566.
[32] Ge L, et al. Improvement of Pine Sawdust Bio-Coke Properties Through Lignin Addition and its Synergistic Effect, SSRN. Available at SSRN 5137698.
[33] Yunos N.F.M, et al. Effect of using Palm Char and Coke as a Reductant in Production of Ferrosilicon. In: IOP Conference Series: Materials Science and Engineering.2020.
[34] Lin X, et al. Insights into the functional group transformation of a Chinese brown coal during slow pyrolysis by combining various experiments, Fuel. 2014; 118: 257–264.
[35] Oh S.Y, et al. FTIR analysis of cellulose treated with sodium hydroxide and carbon dioxide, Carbohydr Res. 2005; 340(3): 417–428.
[36] Chia C.H, et al. Imaging of mineral-enriched biochar by FTIR, Raman and SEM–EDX, Vibrational Spectroscopy. 2012; 62: 248–257.
[37] Zhang H, et al. Promotional effect of NH_3 on mercury removal over biochar thorough chlorine functional group transformation, J Clean Prod. 2020; 257: 120598.
[38] Acquafresca J, Raman spectroscopy on biochar. 2018.
[39] Ferrari A.C, Robertson J, Raman spectroscopy of amorphous, nanostructured, diamond–like carbon, and nanodiamond. Philos Trans R Soc Lond A Math Phys Eng Sci. 2004; 362(1824): 2477–2512.
[40] Sparavigna A.C, Pyrene and Biochar (Raman Spectroscopy). 2024.
[41] Mallick D, et al. Discernment of synergism in pyrolysis of biomass blends using thermogravimetric analysis, Bioresour Technol. 2018; 261: 294–305.
[42] Rambabu N, et al. Production, characterization, and evaluation of activated carbons from de-oiled canola meal for environmental applications, Ind Crops Prod. 2015; 65: 572–581.
[43] Leifeld J, Thermal stability of black carbon characterised by oxidative differential scanning calorimetry, Org Geochem. 2007; 38(1): 112–127.
[44] Kijo-Kleczkowska A, et al. Comparative thermal analysis of coal fuels, biomass, fly ash and polyamide, Energy. 2022; 258: 124840.